VORTEX-SURFACE COLLISION: 3-D CORE FLOW EFFECTS

Mahalingam, R.[*], and Komerath, N.M.[†]
Georgia Institute of Technology

Radcliff, T.D.[‡], Burggraf, O.R.[§], and Conlisk, A.T.[**]
The Ohio State University

ABSTRACT

The interaction of a strong vortex with a curved surface is a basic problem in fluid mechanics, whose solution is crucial to predicting the flow around a rotorcraft. In past work, the initial stages of the interaction between a rotor tip-vortex and a cylindrical airframe were measured and computed using potential flow concepts followed by boundary layer calculations. This paper presents measurements of the lateral velocity component on the top of the airframe during the vortex interaction. These data are used in the prediction of airframe loading in a time frame far beyond that reported in previous work. The axial velocity in the core of the vortex is substantial and is directed back towards the rotor blade. The vortex core circulation scales with rotor rpm. We show here that the axial velocity plays a major role in the final stages of the collision process. Contours of lateral velocity correspond closely to contours of lateral vorticity from previous work. Core axial velocity during the collision is presented as a function of vortex age. The region of high axial velocity flattens and appears to break in two at the final stages of collision. In the computations, the tip-vortex is modeled as a family of helical vortices, whose strength and initial position are chosen based on experimentally measured core axial velocities. The analytical predictions are compared with experimentally measured vortex propagation and surface pressure.

NOMENCLATURE

Some symbols have multiple meanings. The usage of these symbols should be clear from the context.

a_c Vortex core radius

ABS	Side of the cylinder under the advancing blade side of the rotor disk
Cpinst	Instantaneous Pressure, $(p-p_\infty) / q_\infty$
h	Perpendicular distance from vortex to field point
H	Vertical spacing between rotor hub center and airframe centerline
P	Notation for a field point ; also dimensionless pressure
q_∞	Free stream dynamic pressure
$\vec{r}$	Vector from a field point to a point on the vortex
r	magnitude of $\vec{r}$
R	Rotor radius ; also as defined in equation (4)
RBS	The side of the cylinder under the retreating-blade side of the rotor disk.
U_∞	Tunnel freestream velocity
V_∞	Mean flow velocity in the vertical (y) direction
x	Lateral distance in computations non-dimensionalized by airframe radius
Xb	Streamwise distance from cylinder nose in experiments
y	Vertical distance in computations non-dimensionalized by airframe radius
z	Streamwise distance in computations non-dimensionalized by airframe radius
Zb	Vertical distance from cylinder top surface in the experiments
φ	Circumferential location of points on the surface of the airframe cylinder, measured from the top of the airframe ; also , circumferential coordinate around vortex
Γ	Circulation
μ	Rotor advance ratio, $U_\infty/\Omega R$; also cutoff parameter

---

[*] Graduate Research Assistant, Aerospace Engineering
[†] Professor, Aerospace Engineering
[‡] Visiting Assistant Professor, Mechanical Engineering
[§] Professor Emeritus, Aerospace Engineering
[**] Professor, Mechanical Engineering

Ψ Rotor azimuth in degrees, measured from downstream position

Ω Rotor angular velocity

INTRODUCTION

Prediction of the flow-field of a real helicopter configuration depends in part on the ability to compute the interaction between the rotor-wake and the rest of the components. Progress in the last few years has enabled researchers to understand and compute many of the features of the interaction between a rotor wake and nearby surfaces. This knowledge brings us closer to the long-term goal of being able to compute the flow around a complete rotorcraft configuration. One of the outstanding issues in the general area of tip-vortex-component interaction is the collision of the tip-vortex with the airframe surface and what happens thereafter. The interaction of a vortex with a solid body depends on the relative sizes and orientation of the vortex and the body. We consider the case where the scale of the vortex is much smaller than the body scale. The "collision" is defined as a physical process in which the vortex core structure is permanently altered, either locally or globally. We have seen in the past that this collision involves very sharp pressure gradients, as well as unsteady 3-D separation. Despite the apparent complexity of this flow, it has proved to be amenable to analytical prediction, with good agreement achieved between the predictions and experimental results through the initial stages of the vortex-surface collision.

To predict the processes during the latter part of the collision, the vortex structure must be accurately represented. All but one of the previous computations by the current authors and virtually all rotor codes neglect the changes in vortex core structure during the collision. Experiments have shown that the axial velocity component in the core of the vortex is substantial, and plays a critical role in the interaction. We present measured data on lateral velocities in a vertical plane on the top of the airframe, essentially in the same direction as the core axial velocity in that plane. These measurements are used in analytical predictions of the pressure field which incorporate the effects of a variable vortex core and large core axial velocity. The experiments are then extended to illustrate other phenomena present during the interaction.

Previous Work

The trajectories of the tip-vortex have been calculated assuming potential flow outside the vortex[1,2,3] and experimentally documented[4]. The unsteady pressure field around the cylinder has been measured by Brand[5] and Kim[6]. Liou[7] measured the streamwise and vertical components of velocity in a vertical plane on top of the cylinder and along a few streamwise lines on the RBS. Experiments at Georgia Tech and computational efforts at The Ohio State University have been able to isolate details of the first order phenomena associated with the interaction at the front part of the airframe, while work at the University of Maryland has focused on the rear of the airframe[8,9].

Researchers at The Ohio State University[10] have used a three dimensional interacting boundary layer approach to treat the boundary layer flow due to the tip-vortex using data from the Georgia Tech model as a starting point[11]. They were able to predict the development of a secondary vortex and correlate its pressure signature with experimental results. However, these computations were limited to the initial stages of the interaction due to the singular nature of the boundary layer equations for this flow. Affes et al.[3] computed the vortex trajectories in the absence of axial flow and for a fixed core radius. Lee et al.[12] postulate that the collision process is essentially inviscid and characterized by vorticity redistribution by convection causing the reduction of the suction peak on the top of the airframe seen in experiments within 1 ms (12° of rotor azimuth at 2100 rpm). Radcliff et al.[13] have gone a step further to actually model the core-flow using a helical vortex formulation which automatically incorporates axial flow in the vortex. They have focused on the case where the vortex geometry is symmetric with respect to the airframe. This basic core model along with the velocity measurements described in this paper are now being used to compute the present results. The velocity measurements presented in this paper are more accurate because the higher power laser enabled us to track scattering from smaller particles in the core, thus getting closer to the center of the vortex-core.

The substantial role of the core axial velocity, postulated from pressure data on the airframe, is now confirmed by the lateral velocity measurements described in this paper. The axial velocity in the core is seen to persist well beyond 180° of vortex age. Both the tip vortex core and the inboard vortex sheet have substantial wake-like velocities. During the collision, the axial velocity measured at the top of the airframe persists even after the flow has stagnated on the ABS, further evidence of the blade-wake genesis of this flow. Thus, suction peaks on the RBS stay for a long duration.

Capturing the dynamic nature of the axial flow during the interaction is a significant advance in understanding the entire flow field during and after the collision. There has been considerable debate regarding the magnitude and direction of axial velocity in the vortex

core. Recently, vortex measurements using a 3-component laser velocimeter at the University of Maryland[15] on a single-bladed rotor in hover found wake-like axial velocity in the core, but the measured velocity profiles appeared to die out very rapidly within the first 90 degrees of wake age. McAlister[16] measured velocity profiles in the near wake and found a strong wake-like axial velocity along with a weaker jet like velocity. From what is known to date, the development of the axial velocity in the vortex core appears to be a function of a number of factors, primary being the boundary layer roll-up near the blade tip and the no-slip condition at the blade. Resolution of these observations is needed to form general models for vortex interaction with the airframe. It appears that with these issues resolved, the vortex-airframe interaction can be understood and computed to a surprisingly detailed level.

SCOPE OF PRESENT WORK

The latest experiments consist of lateral velocity measurements in the interaction region, in the vertical plane on top of the cylinder. These are matched with lateral vorticity contours obtained by Liou[7], and issues related to core axial velocity are discussed. Core flattening seen from the velocity measurements is described. Predictions of vortex trajectories, core radius and surface pressure are made, incorporating effects of core axial velocity in the model. These are compared with measurements.

Experiments

The experiments were carried out in the J. J. Harper low-speed wind-tunnel at the Georgia Institute of Technology. The rotor is 2-bladed, untapered, with a NACA0015 section. The test configuration is drawn in Fig.1 and the test conditions are listed in Table.1. The advance ratio for all the experiments was 0.1. For the pressure measurements, the rotor rpm was doubled, keeping the advance ratio constant to get enough response out of the microphones. The figures in parentheses indicate the different conditions when used. Note that the flow field scales as rpm if the advance ratio is kept constant. Simple scaling arguments and earlier measurements regarding the scaling have been validated by measurements. The rotor system and support structure are detailed in Ref. 4.

Table 1: Test Conditions
_____

U_∞	5 m/s ± 0.25% (10m/s)
Rotor rpm	1050 ±1 (2100)
Collective pitch	10°
Rotor diameter	0.9144 m.
TPP pitchdown	4.2° ± 0.1°
Vortex strength	0.5 m²/s ± 10% (1 m²/s)
Airframe diameter	0.137 m
Rotor hub height above a/f	0.0685 m
Re at Xb/R=0.52	80,000 ± 10% (160,000)
B.l. thickness at Xb/R=0.52	~ 7 mm

_____

Images of the flow, seeded with smoke from decomposing wax and illuminated for 50 nanoseconds by a pulsed copper vapor laser sheet, were captured using two intensified video-cameras with a variable delay ($\geq$ 10 microseconds) between the two shutters. The surface pressure results compared here are from Ref. 5 and the details of the pressure measurement are described there. Velocity was measured, one component at a time, using an LDV system powered by a 7-watt Argon-ion laser. Light was collected in the back-scatter mode. The lateral component of velocity was measured using a fiber optic probe embedded within the airframe. The laser beams were projected through a hole of 10mm diameter. The quartz window covering the beam aperture on the airframe surface window had to be removed to improve signal-to-noise ratio. Analysis of the results shows that the cavity left by the open window had no significant effect on the vortex behavior above the airframe boundary layer. Fig. 2 shows the measurement grid and fiber-optic probe setup.

The larger solid angle of light collection enabled by the fiber optic probe enabled core velocity measurements. Data at several locations were checked for repeatability. In most of the measuring grid shown, the data rate was high enough (several hundred per second) to enable collection of 50,000 individual points per measuring location. The data were resolved into 1° bins of rotor azimuth, and ensemble-averaged. In the collision region, the data rates fell below a hundred per second, and the number of points was reduced to 25,000.

Computations

In order to predict the experimental results, it is necessary to model the behavior of the vortex when it is in close proximity to the airframe. The modeling employed to accomplish this has four components: a model for the three-dimensional velocity field caused by the vortex, a model for the zero normal velocity boundary condition imposed by the airframe cylinder, a representation of the mean flow away from the airframe, and a means to propagate the vortex based on the predicted velocity field.

Vortex Model

Considerable analysis has been performed to predict the propagation of a vortex near an airframe using a line vortex model described by the Biot-Savart law modified by a cutoff parameter μ to prevent infinite propagation speed as the vortex becomes curved[17,18]. The differential velocity at a point in the cylindrical coordinate system with origin at the center of the airframe(Fig.3) is given by the Biot-Savart law in non-dimensional form is then

$$d\vec{v} = \frac{\vec{\Gamma} x \vec{r}}{4\pi (r^2 + \mu^2)^{3/2}} \, ds \qquad (1)$$

where $\vec{\Gamma}$ is the circulation vector and $\vec{r}$ is the vector from ds to the field point. The cutoff parameter, related to the core radius a_c by the expression $\mu = a_c \, e^{-3/4}$, is based on producing the correct propagation speed for a ring vortex[18]. A fixed-core radius rotor-tip vortex model of this type has been applied to calculate the vortex trajectory in the potential flow surrounding a cylindrical airframe[3]. The results indicate that when the vortex is more than one core radius away from the airframe, the modified vortex model given above is capable of predicting the experimental vortex trajectory and the pressure on the top of the airframe with reasonable accuracy. During this time period the pressure distribution on the body is not substantially influenced by the local properties of the vortex, such as the core radius or the axial velocity in the core. As the vortex moves closer to and finally collides with the airframe, however, the simple vortex model does not predict the airframe pressure distribution data. These experimental results[5,6] show that, as the vortex collides with the airframe, the effect on the advancing blade side is a diffuse positive pressure region while a sharp suction peak persists on the retreating blade side.

The tip-vortex shed from a helicopter rotor blade is typical of all tip vortices shed from wings in that there is present within the core a significant velocity oriented along the generators of the vortex which we term the axial flow within the vortex. Radcliff et al.[13] postulate that the features of the airframe pressure distribution mentioned above are induced by this axial-flow component of the velocity in the vortex. To see how the axial flow is generated, consider that the tip-vortex may be represented by a distribution of vortices wound helically along an infinite cylinder, as illustrated in Fig. 3. Let $d\Gamma$ be the vector circulation of a helical vortex of differential length which can be resolved into axial and azimuthal components in the local cylindrical coordinate system (x', r, ϕ') whose axis is the vortex centerline. We see then that the complete helico-cylindrical vortex sheet can then be resolved into a superposition of axially-oriented line vortices distributed about the core radius a_c and

azimuthally-oriented ring vortices distributed along the cylinder axis. The line vortices induce an azimuthal flow while the vortex rings induce radial and axial flow. The following is an abbreviated derivation of the velocity field. Additional details are given in Radcliff et al[13] although somewhat different notation is used there.

Let us first consider the vorticity associated with the distribution of line vortices. Each line vortex in the distribution about the helical vortex core radius can be represented by the modified Biot-Savart law. Integrating over the core radius gives an azimuthal velocity component v_ϕ evaluated in terms of the complete elliptic integrals of the first and third kind; however, a simpler model will suffice. If we let the core radius approach zero, the distribution of vortices will collapse into a single line vortex with a core radius represented by the cutoff parameter μ. The azimuthal velocity at a field point $P(x , h , \phi)$ measured from the vortex centerline induced by a semi-infinite vortex is then

$$v_\phi = \frac{\Gamma}{4\pi\sqrt{h^2 + \mu^2}} \left(1 + \frac{x}{\sqrt{x^2 + h^2 + \mu^2}} \right) \qquad (2)$$

where, x is the axial distance from the end of the vortex and h is the perpendicular distance from the vortex to point P. This is equivalent to equation (1) integrated along a semi-infinite vortex.

Turning now to the azimuthal component of the helical vortices, which we view as a collection of circular vortex rings distributed uniformly along the vortex cylinder axis, we again proceed from the Biot-Savart law. Consider a differential element of the surface vorticity in the form of a rectangle with length dx and width $ds = a_c \, d\phi'$, located at (x', a_c, ϕ') in the cylindrical-polar coordinate system of the vortex-cylinder. Then for an object point $P (x , h , \phi)$, the modified Biot-Savart law for this element of circulation has the vector form

$$d\vec{v} = \frac{\vec{\gamma}_\phi \times \vec{R}}{4\pi R^3} \, dxds \qquad (3)$$

where, $\gamma_{\phi'}$ is the vector circulation of the ring vortices per unit length along the vortex-cylinder and R is the μ-modified magnitude of the vector from the differential vortex element to the object point P:

$$R^2 = (x - x')^2 + h^2 + a_c^2 + \mu^2 - 2\, a_c \, h \cos(\phi - \phi') \qquad (4)$$

Note that here the cutoff parameter represents the distribution of vorticity about the minor radius of the vortex rings rather than about the major radius a_c. The

cutoff parameter for the rings is assumed to be given by $\mu = a_c\,e^{-3/4}$, the same expression applied to the modified line vortex.

The velocity induced by the vortex rings may also be evaluated in terms of the complete elliptic integrals, however, simple analytical formulas exist for the case where the ring major radius becomes small. To evaluate the velocity in the case where a_c approaches zero (while holding μ fixed), the integrands are expanded in series of powers of a_c/h , keeping only the leading non-vanishing term in the integral. This derivation[13] results in the following components of velocity.

$$v_r = \frac{-\gamma_\phi a_c^{\,2} h}{4(x^2 + h^2 + \mu^2)^{3/2}} \qquad (5)$$

$$v_x = \frac{\gamma_\phi a_c^{\,2}}{4}\left\{\frac{2\mu^2}{(h^2 + \mu^2)^2} + T\right\} \qquad (6)$$

where,

$$T = x\frac{(2\mu^2 - h^2)(h^2 + \mu^2) + 2\mu^2 x^2}{(h^2 + \mu^2)^2 (x^2 + h^2 + \mu^2)^{3/2}}$$

These limit forms, which we term the ringlet velocity distribution, are useful provided the vortex circulation Γ and the quantity $\gamma_\phi a_c^2$ are held fixed, equal to their values for the original cylindrical vortex sheet. This implies that the vortex axial velocity component will increase as the vortex core radius decreases. Note that the parameter μ has become the effective major radius of the ringlet vortices as well as the effective core radius of the modified central line vortex.

The semi-infinite helical vortex velocity distribution is thus given by Equations (2), (5) and (6) for the case where $a_c \rightarrow 0$. A finite segment of such a vortex may then be produced by superposition of two semi-infinite vortices with opposite sign.

Airframe Model

The airframe is modeled using a source-panel method identical to that described by Xiao et al[19] and originally due to Hess and Smith[20]. The airframe is represented by a finite-length circular cylinder which is approximated by $M \times N$ rectangular source panels, where M is the number of panels along the cylinder and N is the number of panels around the cylinder. The panel size is not uniform and is designed to be smallest in the region immediately under the vortex at the top of the cylinder.

The length of the panels in the axial direction vary according to

$$\Delta L_{Vk} = \Delta L_{Vmin} + Bm^2, \text{ for } m = 1 \text{ to } M/2 \qquad (7)$$

where,

$$B = 6\left[\frac{L_{Vmin} - \dfrac{M}{2}\Delta L_{Vmin}}{\dfrac{M}{2}\left(\dfrac{M^2}{2}+1\right)}\right] \qquad (8)$$

ΔL_{Vk} is the length of the mth panel, ΔL_{Vmin} is the minimum panel width and L_{Vmax} is the half length of the airframe cylinder. The panel distribution in the azimuthal direction is also not uniform and is clustered near the symmetry plane at the top of the cylinder. The minimum panel width in the azimuthal direction is $1°$.

The panel mesh is translated axially to maintain the narrowest panels directly beneath the head of the approaching vortex, a strategy required by the close approach of the strong vortex to the airframe. Since the panels are reconstructed in the same configuration, the matrix of influence coefficients which is inverted to find the panel source strengths is independent of time and need not be recalculated at each time step. The panel representation for the airframe is also shown in Fig.3.

Mean Flow Model

The mean flow in the rotor downwash region occupied by the tip-vortex is very complex. Analysis of the vortex trajectory experimentally determined by Liou[7] at Georgia Tech suggests that the mean flow components in the rotor downwash near the airframe could be represented by a constant mean flow with a linear shear, as

$$U_\infty(x) = Ax + B$$
$$V_\infty(x) = Cx + D. \qquad (9)$$

Affes et al.[3] estimated the constants A,B,C,D from the experimental vortex trajectory at points as far as possible from the airframe (approximately $5\ a_c$). This linear model is applied here.

Vortex Propagation Model

To calculate the vortex trajectory, the velocity in the local vortex and panel coordinates are first transformed into the global coordinates. The vortex segments are then advanced by solving the differential equation:

$$\frac{d\,\vec{x}_v}{dt} \;=\; \vec{u} \tag{10}$$

where x_v is the vortex position vector in the *global* coordinates, t is the time, and u is the velocity vector at a vortex segment due to other vortex segments, the presence of the cylindrical airframe, and the mean flow. An Adams-Moulton method is used to calculate the motion of the vortex. The core radius for each vortex segment is evaluated by assuming that segment core volume is conserved as the vortex segment stretches. Vortex segment axial velocity and cutoff parameter are calculated at each time step based on changes in core radius.

Pressure Calculation

Airframe pressure loading is calculated by solving the Euler equations over the surface. The nondimensional axial pressure gradient is given by

$$-\frac{\partial P}{\partial z} = \frac{\partial w}{\partial t} + (w - c)\frac{\partial w}{\partial z} + \frac{v}{r}\frac{\partial w}{\partial \theta} \tag{11}$$

where, w and v are surface speeds in the axial and azimuthal direction and c is the translational speed of the panel mesh. Note that $P = 0.5* Cpinst$. Equation (11) is integrated in z along a line of constant θ; in particular, the axial derivative is integrated from $z = -L$ to z analytically

$$\int (w - c)\frac{\partial w}{\partial z}\,dz = \frac{1}{2}(w^2 - w^2_{-L}) - c(w - w_{-L}) \tag{12}$$

where, $w_{-L} = w(\theta, -L)$

and $2L$ is the length of the computational domain. The time and the azimuthal derivatives in the Euler equation for the pressure are evaluated by central differencing and then integrated using the trapezoidal rule.

RESULTS

Experimental Results

1. Scaling Issues

The lateral velocities presented in this paper were made at 1050 rpm, while the vorticity contours and the surface pressures are at 2100 rpm. To confirm scaling with rpm, the u-component was measured along a vertical line on top of the airframe at 1050 rpm. The core radius(a_c) and maximum circumferential velocity(V) was obtained from the u-velocity profile and was used to compute the circulation as $\Gamma = 2\pi\, a_c\, V$. This gave a vortex core circulation of ~0.5 m^2/s, which is half of what was measured at 2100 rpm. It has also been shown from

McAlister's measurements[16] that the core axial velocity scales with rpm. So the core axial velocity was scaled by a factor of 2 when computations were made for the 2100 rpm case.

2. Wake geometry at interaction

Using flow-visualization and surface pressure plots around the cylinder the geometry of the vortex wake during the interaction was reconstructed. Fig.4. shows a schematic of the rotor wake just prior to collision on top of the airframe. The age of the tip vortex when it interacts on top of the cylinder is confirmed to be about 240°. As the vortex convects down the cylinder it ages to beyond 360°. The inboard sheet rolls up into a counter-rotating vortex, but convects down much faster than the tip-vortex, so the sheet from the newest blade interacts with the older vortex. The inboard sheet is not shown here for the sake of clarity. Also note the distortion of the wake at the rear of the airframe as observed in Ref. 7. The vortex filament at the front of the airframe near an age of 225° is approximately what Fig.3 represents.

3. Velocity Measurements on top of airframe

Fig.5 shows the lateral velocity and vorticity contours at two rotor azimuths on top of the cylinder surface. The three velocity components are individually measured and ensemble averaged over about 100 rotor revolutions. The periodicity and repeatability of the flow, which makes this possible, are confirmed by the excellent correlation obtained between the lateral vorticity contours constructed from the data taken in 1987 by Liou[7], and the lateral velocity contours obtained by Mahalingam[14] in 1997. This obviates the need for simultaneous 3-component measurement in this flow.

While the swirl velocities in the wake approach 2-3 m/s (4-6 m/s at 2100 rpm) in most parts, a predominant feature is the high core axial velocity, directed toward the blade. Note the persistence of the axial velocity even after the maximum vorticity has died down. A high magnitude of core axial velocity is seen throughout and beyond the interaction averaging about 12.5 m/s (25 m/s at 2100 rpm). This is the value that has been used in the computations. The vortex center matches up very well when seen as the point of maximum lateral velocity and vorticity.

4. Effect of vortex age on core-axial velocity

Fig. 6 shows the maximum axial velocity measured in the core as a function of vortex age. The rapid variation seen in the axial velocity may be in part due to the inablility to measure velocities in the exact center of the core. Axial velocities up to 16 m/s (32 m/s at 2100 rpm) are measured around 240°, which is higher than the peak tangential velocity at that point (~ 20 m/s at

2100 rpm). Note that the axial velocity in the core even at 270° vortex age is of the order of 10 m/s (20 m/s at 2100 rpm). Even this late into the vortex age there is a persistence of the core axial velocity. Since the core axial velocity locally is primarily an effect of the rolled up sheets in the core, this would indicate that the core circulation also has to be very high, until the vortex hits the surface. Beyond that, while the axial velocity in the vortex tube on the RBS (still attached to the rotor blade, but growing older) is still very high, the velocity in the cut filament on the ABS goes down.

These observations suggest that any dissipation / diffusion of the wake strength that are seen in rotor-tip-vortex measurements are just artifacts of inadequate measurements in non-periodic flow-fields. Once a clean, periodic flow-field is established, the rotor-wake is seen to persist far beyond 300° of vortex age.

5. Core flattening on top

The results of previous computations suggest that the core would flatten as the vortex approaches the cylinder. Fig.7 shows the ratio of the vertical to the streamwise dimension of the vortex (called here as the Vortex Aspect Ratio), as it goes through the final stages of the interaction. The core remains circular until the close interaction with the surface begins. At about 258° of vortex age the core abruptly flattens along the vertical dimension and forms into a sheet like region, with a persistence of axial velocity. The core flattening occurs over a rotor azimuth of about 4°, which is much less than 1ms. This is not captured in the vorticity contours since the vertical and streamwise components of velocity were obtained at an azimuth resolution of 6°, thus completely washing over the phenomenon. This issue is to be addressed next in the computations. After flattening the core breaks in two distinct regions, and this phenomenon is being investigated further.

Computational Results

The numerical model of the vortex and airframe has been applied to predict some of the experimental results from Georgia Tech. Vortex trajectory and airframe surface pressure are parameters available for comparison. To perform this comparison, the measured vortex position at rotor angle $\psi = 180°$ was extracted from the experimental data of Liou[7] and used to initiate the computation. This places the vortex about four core radii away from the airframe, where detail of the vortex structure is relatively unimportant.   To enforce the assumption of an infinitely long vortex, the finite vortex end points recorded in the experiments were extrapolated to produce semi-infinite ends. Measured values of vortex circulation, core radius and axial velocity were also incorporated into the initial conditions.   For the computations presented here, experimental and

computational parameters were non-dimensionalized on the airframe radius of 0.137 m and the mean flow velocity of 10 m/s which results from a 0.1 advance ratio. This gives a dimensionless circulation of 2.24, an initial dimensionless core radius of 0.1, and a dimensionless axial velocity in the vortex core of 2.5.

The airframe is represented with 81 axial and 40 azimuthal panels. Once initiated, the vortex was allowed to propagate freely with a time step of 0.002985, corresponding to a rotor phase angle of 0.25°. The computation was halted when one of the vortex centerline points, which define each vortex segment, crossed the airframe boundary in violation of the zero normal velocity boundary condition. The sensitivity of these results to number of panels and vortex segments, airframe and vortex length, and time increment has been tested. Doubling the number of panels or vortex segments, or increasing the airframe or vortex length, has little effect on the results. Four digit accuracy is obtained for vortex trajectory and two digit accuracy is obtained for pressure at the times presented. Time step size is chosen to ensure that vortex movement does not exceed the narrowest panel width in any interval, so time steps are typically shortened as the vortex approaches the airframe. Decreasing the time increment further has little effect other than providing finer resolution of the exact time at which the vortex is predicted to penetrate the airframe.

The predicted results for vortex trajectory are shown in Fig. 8 from $\psi = 190°$ to 260° in 10° increments along with the measured trajectory from Liou[7] at $\psi = 210°$ and 240°. The trajectory matches well over 30° of rotor advance but the experimental vortex moves toward the cylinder more rapidly than the modeled vortex over the next 30°. These results also compare well with the with the results of Affes et al.[3] for the predicted vortex trajectories until $\psi = 240°$. Affes et al.[3] used a fixed core radius and no axial velocity. However the computation of Affes et al.[3] is much more computationally intensive than the current computation. Moreover, the present computations can be extended beyond those of Affes et al[3]; indeed, the results at $\psi = 250°$ and 260° show that the advance of the vortex is halted. This has been seen in previous experiments[4,7] and in the current visualizations at about the same time as in the current computations.

The time variation in core radius at each vortex segment is shown in Fig.9. This figure shows that although the trajectory is similar to Affes et al.[3] , axial momentum in the vortex core does cause the vortex to bulge slightly on the advancing-blade side (ABS) of the airframe and to thin substantially on the retreating-blade side (RBS). At the high value of axial velocity used here, the radius nodes can become numerically unstable. Very small mismatches in vortex segment radius tend to excite

numerical oscillations and wave propagation, as seen in the figures. This tendency can be partially controlled by careful selection of the segment size, but it does not appear to drastically effect the overall trends of core radius.

On Figs.10-12 are the results for the pressure plotted as a function of z(Fig. 3) for several rotor phase angles at three locations around the cylinder azimuth near the top of the airframe. These locations are the top of the airframe and 15° on either side. Note that for the first two rotor phase angles, the amplitude of the experimental suction peak is greater on the top than elsewhere; the amplitude on the advancing side is lower than that on the retreating side. However, at $\psi=240°$, the experimental suction peak on the top of the airframe is significantly reduced. The computational results are depicted as the solid lines. Note that the computational results are in reasonable agreement with experiment except right on top of the airframe at $\psi=240°$. Here the pressure is substantially reduced from its value at $\psi=222°$; the axial flow acts to reduce suction on the top and RBS of the airframe. This effect just begins to show up at $\psi=240°$ and increases rapidly in importance through $\psi=260°$, when compared to the no axial-flow results period. It is likely that the significant reduction is partially due to core deformation as seen in the experiments on Fig. 7. Note that in the perpendicular interaction described in Lee et al[12], a similar reduction in pressure occurs rapidly as a result of the presence of axial flow in the vortex. However, the present problem is more complex geometrically and the deformation of the vortex core is likely to be play a significant role locally in time. This effect is presently being incorporated into the computations. Note that no adjustable parameters have been employed in the current computations.

CONCLUSIONS

1. Lateral velocity measurements on top of the airframe correlate well with vorticity contours.
2. Early in the interaction the core axial velocity is higher than the peak tangential velocity.
3. The strong wake-like axial velocity in the core, which persists even after the vorticity in the tip-vortex is going down on top of the airframe, is proposed to be due to the connectivity of the filament on the RBS to the rotor blade.
4. The vortex-wake persists in strength beyond 300 degrees of vortex age.
5. Core flattening, as suggested from earlier computations, has been captured experimentally in the final stages of the interaction on top of the airframe.
6. Computations predict a sharp decrease in core radius on the RBS in the post-collision phase, which can be traced to the axial velocity in the core.

7. Computations also show an increase in core-radius on the ABS, seen in earlier flow-visualization as a bulging of the core.
8. In the later stages of the computation, around $\psi = 250°$ for an advance ratio of 0.1, the vortex advance velocity slows and the vortex advance is actually halted on the top of the airframe. This is also seen in experiments.
9. The computed pressure at $\psi=240°$ on the top of the airframe severely underpredicts the experimental results. This issue is being addressed presently and is likely due to the lack of a core deformation model. The advancing side pressures are well predicted at $\psi=222°$ and $\psi=240°$.

REFERENCES

1. Scully, M.P, "Computation of Helicopter Rotor Geometry and Its Influence on Rotor Harmonic Airloads, M.I.T. Aeroel.& Struc. Res. Lab. Report, ASRL TR 178-1, March 1975.
2. Egolf, T.A., and Landgrebe, A.J., "Helicopter Rotor Wake Geometry and Its Influence in Forward Flight", NASA CR 3726, October 1983.
3. Affes, H., Conlisk, A.T., Kim, J.M. and Komerath, N.M.,"A Model for Rotor Tip Vortex-Airframe Interaction, Part 2: Comparison with Experiment", AIAA J., Vol. 31, no. 12, pp. 2274-2282, 1993.
4. Kim, J.M., and Komerath, N.M., "Summary of the Interaction of a Rotor Wake with a Cylinder", AIAA Journal, Vol. 33, No. 3, March 1995, p. 470-478.
5. Brand, A.G., " An Experimental Investigation of the Interaction between a Model Rotor and Airframe in Forward Flight", PhD Thesis, Georgia Institute of Technology , 1989.
6. Kim, J.M., "An Experimental Study of the Interaction between a Rotor Wake and an Airframe with and without Flow Separation", PhD Thesis, Georgia Institute of Technology, 1993.
7. Liou, S.G., " Velocity Measurements on a Lifting Rotor/Airframe Configuration in Forward Flight", PhD Thesis, Georgia Institute of Technology, 1989.
8. Norman, T. and Light, J. S., " Rotor Tip Vortex Geometry Measurements Using the Wide-Field Shadowgraph Technique", J. AHS, Vol. 32(2), Apr. 1987.
9. Bagai, A. and Leishman, J.G., "Experimental Study of Rotor Wake/Body Interactions in Hover", J. AHS, October 1992, pp. 48-57.
10. Affes, H., Xiao, Z., Conlisk, A.T., Kim, J.M., and Komerath, N.M., "The Three-Dimensional Boundary

Layer Flow Due to a Rotor Tip Vortex", AIAA 93-3081, July 1993.

11. Mahalingam, R., Peterson, K.G., Funk, R., Komerath, N.M., and Conlisk, A.T., " Recent Experiments on Vortex Colllisions with a Cylinder", AIAA 95-2236, June 1995.

12. Lee, J., Xiao, Z., Burggraf, O.R., Conlisk, A.T., and Komerath, N.M., "An Inviscid Analysis of Vortex-Surface Collisions", AIAA 95-2237, June 1995.

13. Radcliff, T. R., Burggraf, O. R. annd Conlisk, A. T. 1997, "Modelling of the Collision of a Rotor-Tip Vortex with an Airframe", AIAA Aerospace Sciences Meeting, Reno, NV, January 1997, AIAA paper 97-0658.

14. Mahalingam, R. and Komerath, N.M., "Rotor Tip-Vortex/Airframe Collision Features", AIAA 96-2013, June 1996.

15. Leishman, J.G., Baker, A. and Coyne, A., "Measurement of Rotor Tip Vortices Using Three-Component Laser Doppler Velocimetry", AHS Aeromechanics Specialist Conference, October 1995.

16. Mcalister, K.W., "Measurements in the Near Wake of a Hovering Rotor", AIAA 96-1958, June 1996.

17. Batchelor, G. K., Introduction to Fluids, Cambridge University Press, Cambridge, P. 87, 1967.

18. Moore, D.W. and Saffman, P.G., "The Motion of a Vortex Filament with Axial Flow", Philosophical Transactions of the Royal Society, V. 272, pp. 403-429, 1972.

19. Xiao, Z., Affes, H. and Conlisk, A.T., "The Boundary Layer Flow due to a Vortex Approaching a Cylinder", Journal of Fluid Mechanics, V. 275, pp. 33-58, 1994.

20. Hess, J.L. and Smith, A.M. (1967), "Calculation of Potential Flow about ArbitraryBodies", Progress in Aeronautical Sciences, Vol. 8, pp. 1-138, Pergamon, New York.

Upstream View

2.74 m

H/R = 0.3

Camera

Side View

Zb

Xb

U

2.13m
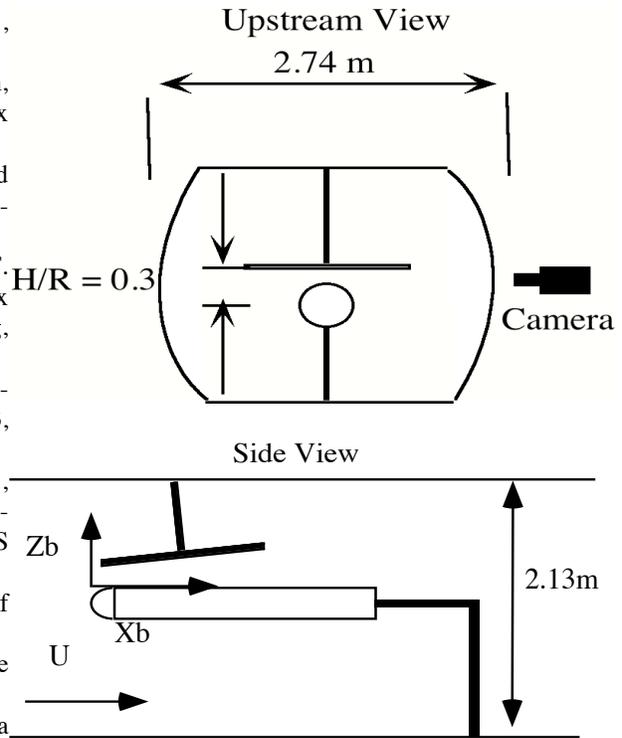
Fig.1. Test Configuration in the Georgia Tech Wind Tunnel

Xb/R =0.352   Xb/R=0.52

Zb/R =0.072

Zb/R =0.011

embedded fiber-optic probe

U

Fig.2. LDV measurement technique and grid

beam crossing measurement volume 1.7 mm by 0.1 mm

embedded fiber-optic probe

Top view

R=0.457m

U
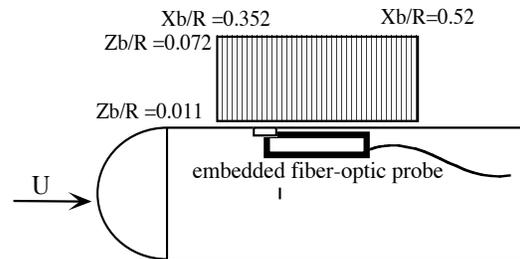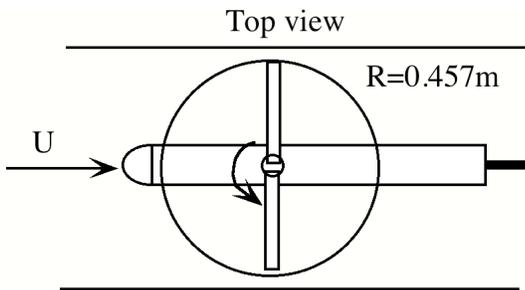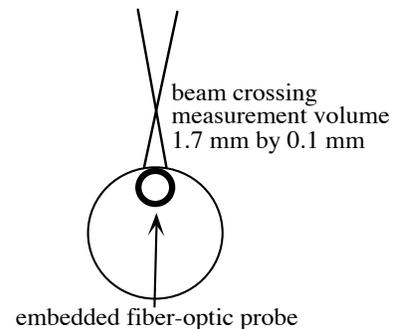
Fig.2.(cont). LDV measurement technique and grid
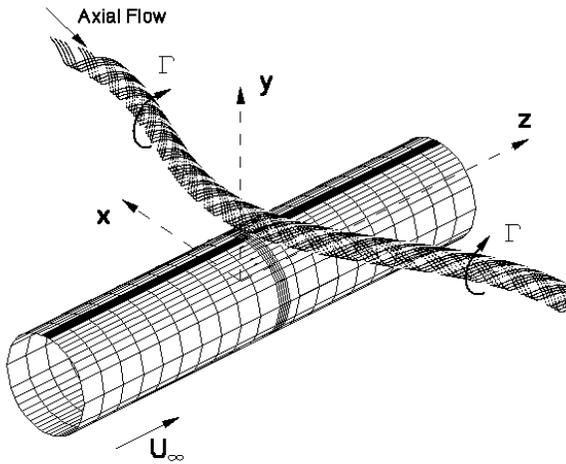
Fig. 3. Panel airframe and helical vortex representations and Coordinate System used for the computations.

● When vortex interacts on top of airframe it is more than 180^0 old

● Experiments : Effect of vortex on Airframe seen until $\sim 600^0$
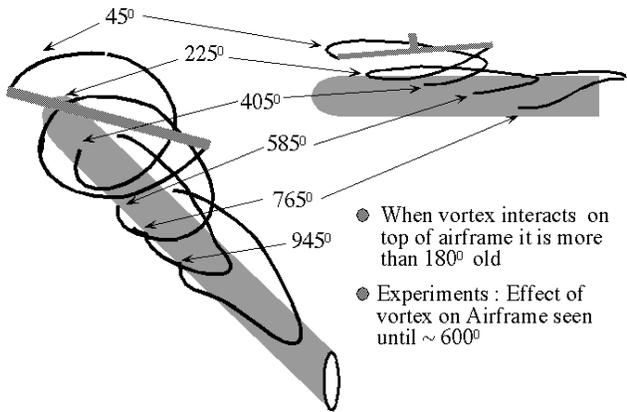
Fig.4. Wake Geometry prior to collision
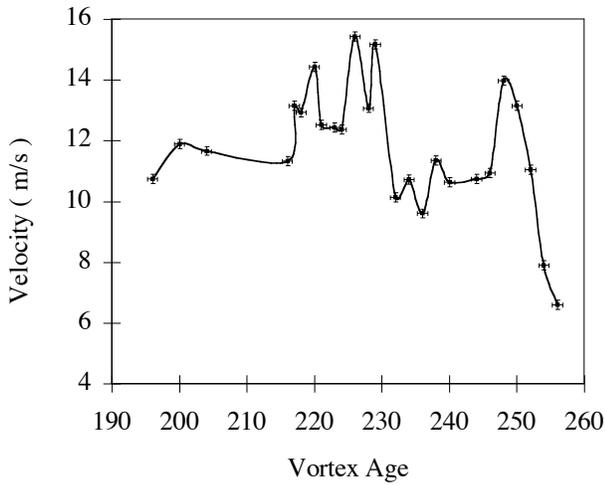
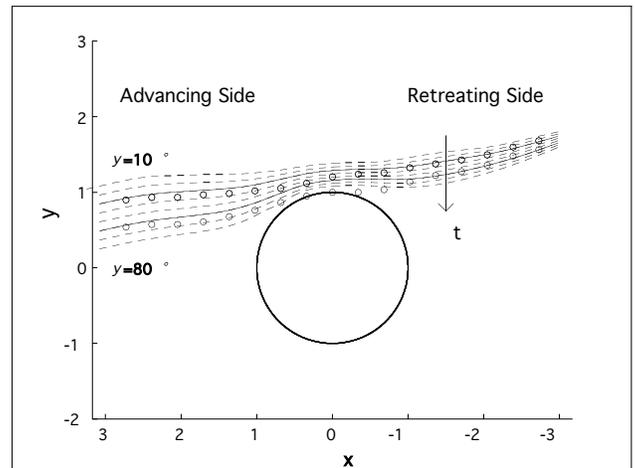**Fig.6. Variation of maximum axial velocity in the tip-vortex core**
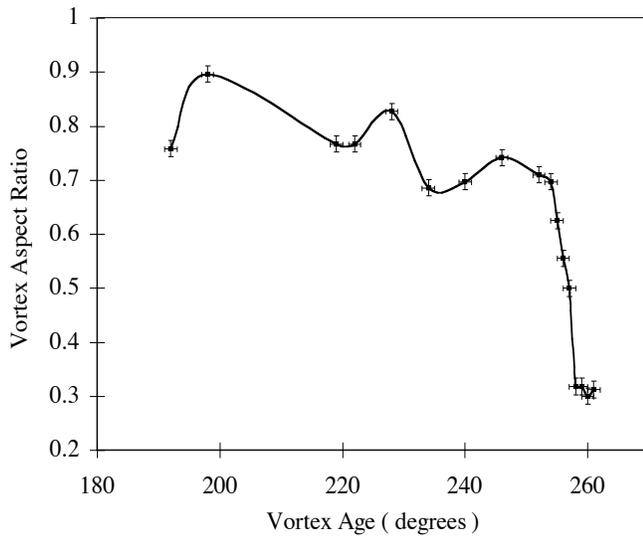
(a) top view

Fig.7. Initiation of core flattening on top of airframe.
The y-axis is defined as the ratio of the vertical to the streamwise dimension of the vortex core
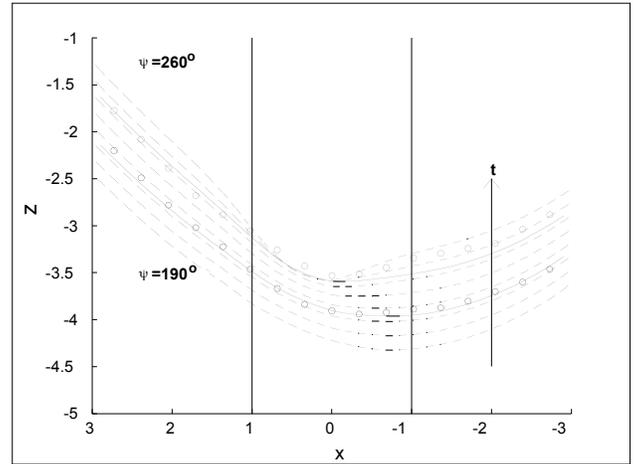
(b) front view

Fig.8. Vortex trajectory from $\Psi=190°$ to $260°$. The solid lines denote computed trajectories at $\Psi=210°$ to $240°$ and the circles denote the experimental data at the same times. The initial position was specified from experiment at $180°$. Arrow denotes increasing Ψ.
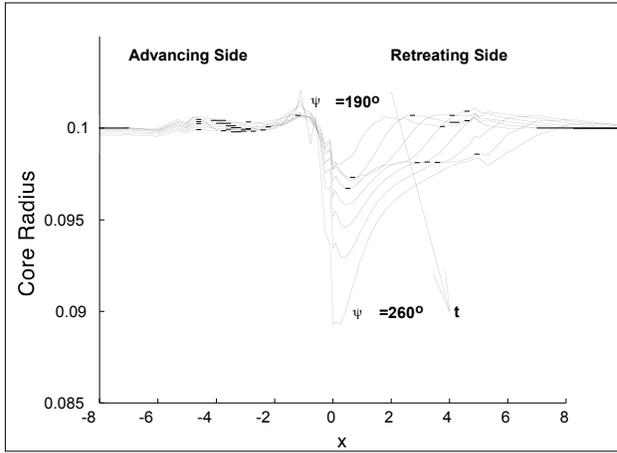
Fig.9. Vortex core radius from from Ψ=190° to 260°. for the condition in fig.8. Note the bulging on the ABS and the thinning on the RBS.
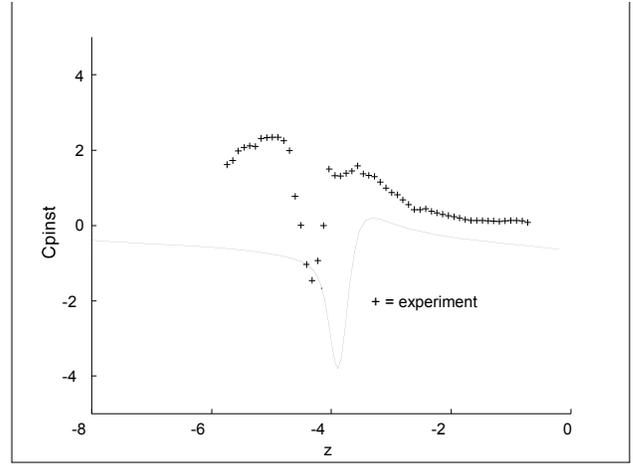
Fig.10(c)

Fig.10. Cpinst as a function of distance along the airframe at ψ=210°. (a) φ=0°; (b) φ=15° to advancing side; (c) ψ=15°to retreating side.
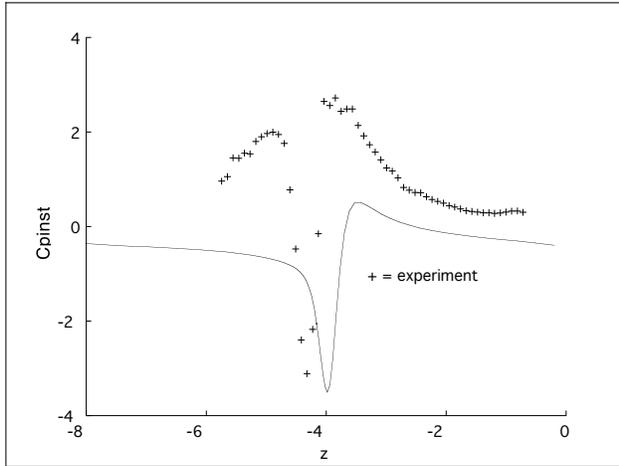
Fig.10(a)
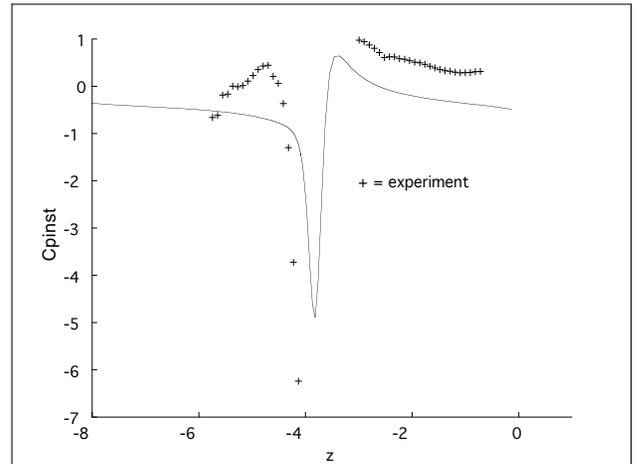
Fig.11(a)

Fig.10(b)

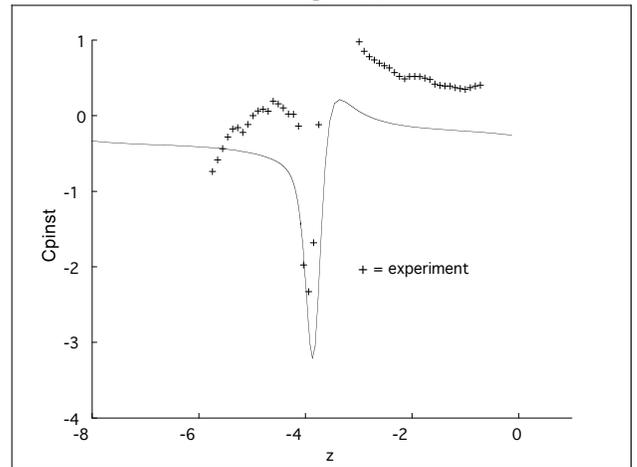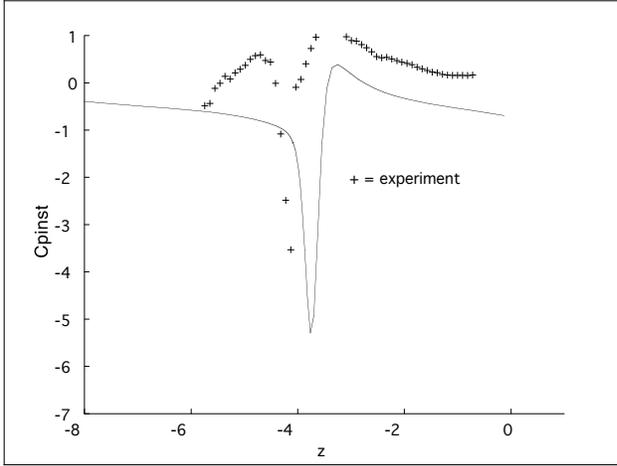
Fig.11 (b)

13
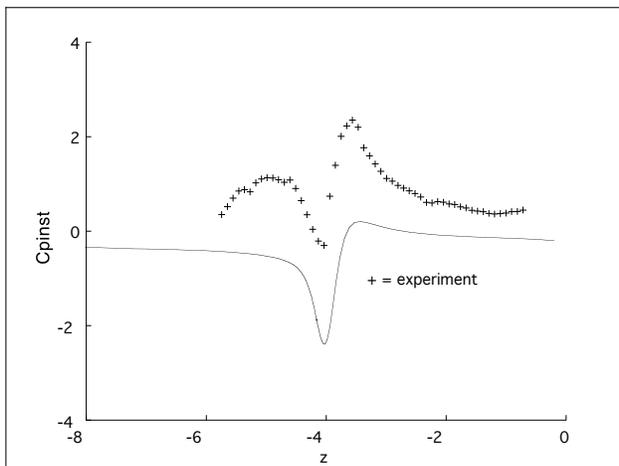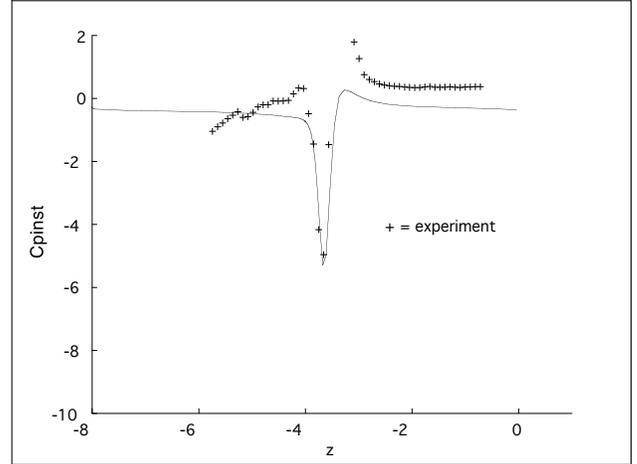
Fig.11(c)

Fig.11. Cpinst as a function of distance along the airframe at ψ=222°. (a) φ=0°; (b) φ=15° to advancing side; (c) φ=15° to retreating side.
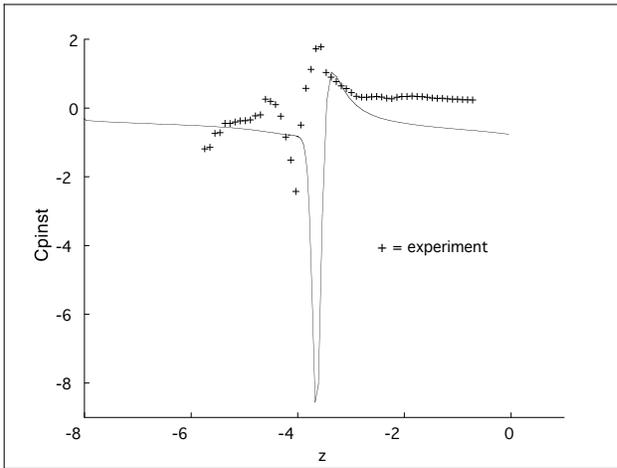
Fig.12(b)
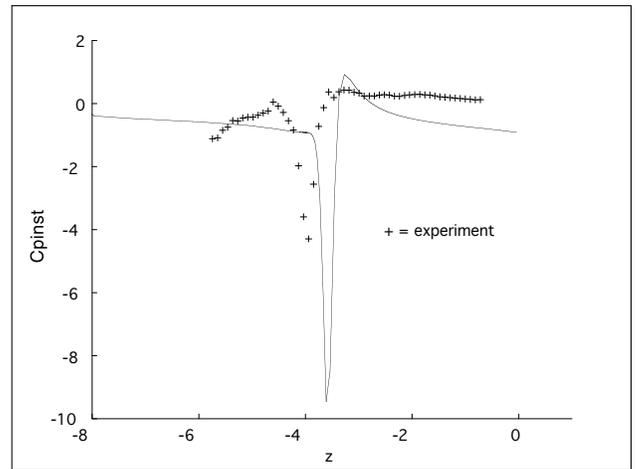
Fig.12(a)

Fig.12(c)

Fig.12. Cpinst as a function of distance along the airframe at ψ=240°. (a) φ=0°; (b) φ=15° to advancing side; (c) φ=15° to retreating side.